Sixth International Symposium on Turbulence and Shear Flow Phenomena
Seoul, Korea, 22-24 June 2009

MIXING OF SEVERAL FLUIDS IN AN ACCELERATED NOZZLE FLOW

Tobias Winnemöller, Matthias Meinke, Wolfgang Schröder
Institute of Aerodynamics,
RWTH Aachen University
Wüllnerstraße 5a, D-52062 Aachen, Germany
t.winnemoeller@aia.rwth-aachen.de

ABSTRACT

The present paper investigates the turbulent mixing of the heavy precursor gas TEOS in a hot accelerated transonic air co-flow. A mass flux of $\dot{m}_{inj,TEOS} = 0.5\frac{g}{s}$ TEOS premixed with $\dot{m}_{inj,N2} = 0.32\frac{g}{s}$ nitrogen is injected in an air co-flow with a mass flux of $\dot{m}_{co-flow} = 100\frac{g}{s}$ at $Ma_{co-flow} = 0.66$ and $T_{co-flow} = 1200K$ and afterwards accelerated to supersonic speed. High frequency, non equilibrium turbulence phenomena dominated by pronounced free shear layers are expected to significantly affect the mixing process. Therefore, a large-eddy simulation (LES) which is capable of capturing the turbulent behavior on the relevant scales is used to simulate the mixing process. An efficient multi-species LES method based on the MILES technique with an explicit 5-stage Runge-Kutta scheme is applied. The results of the simulations show that the wake is dominated by strong vortex shedding from the blunt injector trailing edge. The mixing process is impeded by these primary vortices.

INTRODUCTION

Nanoparticles are broadly used in industry and science. The preferred current methods to synthesize these particles are flame synthesis and hot-wall synthesis. Studies indicate that high heating and quenching rates as well as a homogeneous flow field are the most important parameters for achieving a narrow size distribution and low aggregation of the particles. (Schild et al., 1999)

The project "Gasdynamically Induced Nanoparticles" pursues a new approach to realize an improved production process for nanoparticles. A precursor gas is mixed with an accelerated air flow in a Laval nozzle at transonic co-flow speed. The mixed flow is accelerated to supersonic flow speed and afterwards quasi-instantaneously heated by a shock wave. In the reaction chamber the air precursor mixture reacts and nanoparticles are generated. A second Laval nozzle terminates the reaction by accelerating and hence cooling down the flow. Downstream of the second nozzle the total enthalpy of the flow is reduced by injecting water in a quenching system. The schematic of the facility is depicted in figure 1.

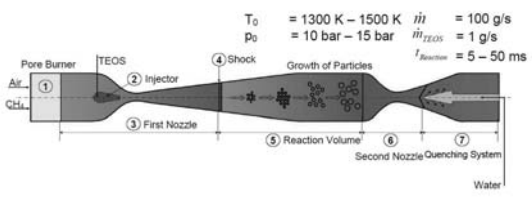

Figure 1: Schematic of the flow facility (Grzona et al., 2007)

As part of this project the mixture of the precursor gas in an accelerated hot air flow is numerically investigated at the Institute of Aerodynamics. A spatially and temporally homogeneous mixture is required to achieve particles of a narrow size distribution and high quality. The high velocity and short mixing time make a rapid mixing necessary. The objectives of the numerical simulations are an improved understanding of the mixing and the parameters defining this process. From this analysis an improvement of the mixing homogeneity and a reduction of the mixing length is to be derived. In addition, based on the ability to predict the mixing process, the impact of changing any part of the overall injection setup on the nanoparticle quality is to be estimated.

The mixing of a gas in a co-flow has been studied for many years due to its relevance for many technical applications. Especially the injection of a propellant in combustion chambers is a frequent application. The research most similar to this project was conducted for RAMJET and SCRAMJET engines. Gerlinger et al. (2008), for example, studied a Mach number $Ma = 2.0$ injection of a propellant for an injector which induced longitudinal vortices into the flow. A significant improvement of the mixing quality due to the induced longitudinal vortices was shown. While this study was conducted using a Reynolds-averaged Navier-Stokes (RANS) method Berglund and Fureby (2007) performed an LES for mixing and combustion in a SCRAMJET combustion chamber which showed good agreement with experiments. Many further studies numerically and experimentally investigated similar cases.

While the overall topic of this paper is similar to those studies in the sense that a gas is mixed in a co-flow, there are significant differences to this study. First of all, the work presented in this paper focuses on the mixture of a gas in a co-flow with a negative pressure gradient. This acceleration of the co-flow has an effect on the mixture, which was not studied in the past. A further difference is that the co-flow possesses a higher velocity than the injected gas, whereas in most jet-in-a-co-flow studies the jet had a higher or at least a similar speed as the co-flow.

This paper is organized as follows. After a description of the flow problem governing equations and the numerical method are discussed, the validation of the multi-species mixing by simulation of a propane jet is presented. Subsequently, the grid configuration and some computational details are shown followed by a discussion of the simulation results and the conclusion.

DESCRIPTION OF THE FLOW PROBLEM

The studied problem of the present paper is a Laval nozzle with a width of 15mm and an overall length of about 200mm. The throat has an area of 15mm times 6mm. The total pressure of the main flow is $p_{0,co-flow} = 10bar$ and

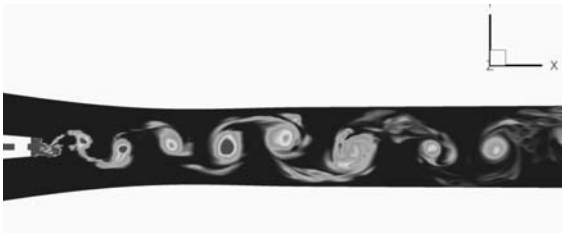

Figure 2: TEOS concentration in the injector wake

the total temperature is $T_{0,co-flow} = 1300K$. An injector with an airfoil like shape, a length of 20mm and a blunt trailing edge thickness of $D_{te} = 1.5mm$ injects the precursor gas TEOS at transonic flow speed. It has six injection holes with a diameter of 0.5mm each. The injected mass flux is about 0.8% of the main flow and has a total temperature of $T_{0,inj} = 650K$. The injection flow speed is $u_{\emptyset,inj} = 100m/s$, which is approximately 1/3 of the velocity of the main flow. Its Reynolds number is $Re = 16000$. The injected gas mixture of Nitrogen and the precursor TEOS is 3 to 7 times denser than air depending on the mixing ratio of TEOS and Nitrogen.

The x-coordinate of the cartesian frame of reference defines the streamwise direction. The origin of the coordinate system is in the center of the nozzle throat such that the exit of the injector, which is located in the subsonic part of the nozzle is described by a negative x-coordinate. The y-coordinate defines the vertical direction and the spanwise direction i, i.e., the direction normal to the sidewalls, is denoted by the z-coordinate.

From the illustration of the TEOS concentration in (Fig. 2) it is clear that strong vortices being shed from the blunt injector trailing edge dominate the wake and the mixing area. The mixing strongly depends on the macroscopic turbulence structure which develops in the wake.

GOVERNING EQUATIONS

The Navier-Stokes equations of a multi-species fluid, i.e. the conservation equations for the partial density ρ_n of $N-1$ species with a total number of N species, are included and approximately solved to determine the flow physics of this problem (Peyret and Taylor, (1983)). The dimensionless conservative tensor notation is

$$\frac{\partial \mathbf{Q}}{\partial t} + \left(\mathbf{F}^{\mathbf{C}}_{\beta} - \mathbf{F}^{\mathbf{D}}_{\beta}\right)_{,\beta} = 0, \tag{1}$$

with $\mathbf{Q}$ representing the vector of the conservative variables

$$\mathbf{Q} = \left[\rho_n, \rho, \rho u_\alpha, \rho E\right]^T, \tag{2}$$

$\mathbf{F}^{\mathbf{C}}_{\beta}$ denoting the vector of the convective, and $\mathbf{F}^{\mathbf{D}}_{\beta}$ being the vector of the diffusive fluxes

$$\mathbf{F}^{\mathbf{C}}_{\beta} - \mathbf{F}^{\mathbf{D}}_{\beta} = \begin{pmatrix} \rho_n u_\beta \\ \rho u_\beta \\ \rho u_\beta u_\beta + \rho \delta_{\alpha\beta} \\ u_\beta \left(\rho E + p\right) \end{pmatrix} + \frac{1}{Re} \begin{pmatrix} j_{n\beta} \\ 0 \\ \sigma_{\alpha\beta} \\ u_\alpha \sigma_{\alpha\beta} + q_\beta \end{pmatrix}. \tag{3}$$

For a Newtonian fluid the stress tensor $\sigma_{\alpha\beta}$ can be written as a function of the strain rate tensor $S_{\alpha\beta}$

$$\sigma_{\alpha\beta} = -2\nu \left(S_{\alpha\beta} - \frac{1}{3} S_{\gamma\gamma} \delta_{\alpha\beta}\right) \tag{4}$$

with

$$S_{\alpha\beta} = \frac{1}{2}\left(u_{\alpha,\beta} + u_{\beta,\alpha}\right). \tag{5}$$

The mass diffusion$j_{n\beta}$ for a dilute mixture can be described by Fick's law

$$j_{n\beta} = -\frac{\rho D_n}{Sc_0} Y_{n,\beta}, \tag{6}$$

where Y_n is the mass fraction of the species n, D_n is the diffusion coefficient computed via mixing rules from the binary diffusion coefficients, $Sc_0 = \nu_0/D_0$ is the Schmidt number, and the subscript 0 indicates the reference state of the mixture. With Fourier' law of heat conduction the heat flux q_β is proportional to the negative gradient of the temperature via

$$q_\beta = -\frac{k}{Pr\left(\gamma_0 - 1\right)} T_{,\beta}, \tag{7}$$

where k is the thermal conductivity of the fluid mixture and Pr is the Prandtl number. The equation of state is used to close the system

$$p = \frac{T}{\gamma_0} \rho \sum_n R_n Y_n = \frac{T}{\gamma_0} \rho R, \tag{8}$$

where γ is the ratio of specific heats, T the temperature, p the pressure, and R the gas constant.

All gas coefficients are assumed to be a function of the temperature, e.g. the dynamic viscosity η is calculated by

$$\ln \eta^*_n = \sum_i a^*_{i_n} \left(\ln T^*\right)^{i-1}, \tag{9}$$

where the superscript * denotes dimensional values.

NUMERICAL METHOD

The governing equations are discretized using a central-upwind AUSM (advective upstream splitting method) scheme, i.e., the inertia terms are approximated using an upwind-based scheme and the pressure terms are discretized with a centered low dissipation stencil. The large-eddy simulation (LES) method is based on the MILES (monotone integrated LES, Fureby and Grinstein (1999, 2002)) technique to represent the effect of the unresolved subgrid scales (SGS). The intrinsic dissipation of the numerical scheme is assumed to transfer energy from the large to the small scales and serves as an implicit SGS model.

An explicit 5-stage Runge-Kutta method is used for time integration. The solution vector Q is propagated in time from time level n to time level $n+1$ by

$$\mathbf{Q}^i = \mathbf{Q}^n + \alpha_i \Delta t \mathbf{RHS}\left(\mathbf{Q}^{i-1}\right). \tag{10}$$

For time-level t^{n+1} this results in

$$\mathbf{Q}^{n+1} = \mathbf{Q}^5. \tag{11}$$

The superscript i represents the Runge-Kutta step index $i = 0, ..., 5$, while n indicates the time level. The quantity Δt is the time step and **RHS** is the known residual at the previous Runge-Kutta step. The Runge-Kutta coefficients are optimized for stability of a centrally discretized scheme. They are $\alpha_i = \left(\frac{6}{24}, \frac{4}{24}, \frac{9}{24}, \frac{12}{24}, \frac{24}{24}\right)$.

Due to significant differences in species density, $\rho_{TEOS} \approx 7\rho_{air}$, large gradients in the injection area occur. To improve the stability and increase the convergence rate of the scheme an artificial diffusivity is introduced. The approach is similar to that discussed by Fiorina and Lele (2007), which was based on an approach by Cook and Cabot (2005). Unlike the derivative of the entropy which has been used as stability sensor the derivative of the entropy a derivative of the mass

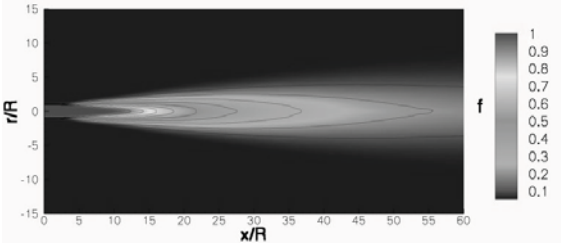

Figure 3: Contours of the mean mixture fraction f in the jet symmetry plane, Renze et al. (2008)

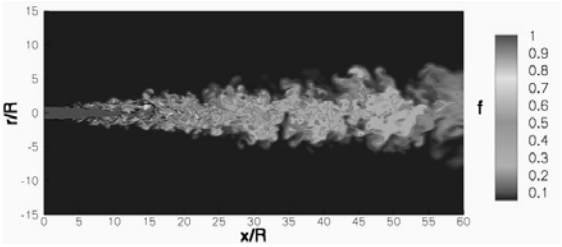

Figure 4: Contours of the mixture fraction f at an instantaneous time level, Renze et al. (2008)

fraction of TEOS was taken as indicator for areas causing stability problems in this study. The artificial diffusivity term which is added to the physical diffusivity reads

$$D_{art} = c_{art} \left(\Delta x\right)^4 \left| \frac{\partial^3 Y_{TEOS}}{\partial x^3} \right|, \qquad (12)$$

where c_{art} is a constant to adjust the value of the artificial diffusivity D_{art}.

VALIDATION

The described numerical method has been validated by simulating a propane (C_3H_8) jet in an air co-flow, and comparing the numerical data with experimental results of Schefer and Dibble (2001). Laser Rayleigh scattering was used in their experiments to generate time- and space-resolved measurements of the species mixture field. Earlier investigations by Dibble et al. (1987) provide corresponding velocity data.

The jet at a Reynolds number of $Re_{jet} = 68000$ based on the jet diameter and a jet bulk velocity of $u_{jet} = 53\frac{m}{s}$ is injected into an air co-flow at a velocity ratio of $\frac{u_{jet}}{u_{co-flow}} = 5.75$. The simulation is done on a structured grid with 13 blocks and 3.5 million grid points. The smallest grid spacing in the shear layer is $\Delta r_{min} = 0.042 R_{jet}$, where R_{jet} is the radius of the jet. The smallest mesh spacing in the streamwise direction is $\Delta x_{min} = 0.13 R_{jet}$.

Figure 3 shows the time-averaged mixture fraction f. On the centerline the maximum value of unity is preserved for twelve jet radii. This point marks the end of the potential core. The instantaneous mixture fraction is shown in figure 4. Instabilities develop shortly downstream of the inlet. They are triggered by an inflow forcing which induces randomly updated vortical rings into the flow as suggested by Bogey et al. (2002). Downstream of $\frac{x}{R_{jet}} = 12$ the transition to a fully turbulent state is visible. The experimental data provided by Schefer and Dibble (2001) allows a detailed comparison with the prediction of the turbulent mixing by the jet simulation. The centerline mixture fraction decay

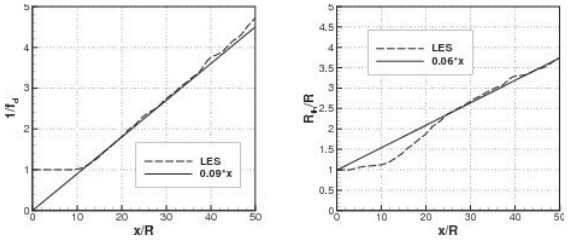

Figure 5: Left: reciprocal mean mixture fraction f along the centerline, right: mixture fraction half-radius R_{fh} of a turbulent non reacting C_3H_8 jet, Renze et al. (2008)

	C_1	C_2
LES, Renze et al. (2008)	0.09	0.06
Experiments, Schefer and Dibble (2001)	0.08	0.06

Table 1: Numerically and experimentally determined constants of the mean flow field.

for non-reacting turbulent jets can be correlated with the distance from the virtual origin $x_{0,1}$ using a linear function

$$\frac{1}{f_{cl}} = C_1 \left[(x - x_{0,1})/R\right], \qquad (13)$$

where C_1 is the centerline decay constant and $x_{0,1}$ is a virtual origin, which is defined by the location of the onset of an approximately constant slope. The reciprocal mean mixture fraction f along the centerline is plotted in Fig. 5. It is evident that the centerline mixture fraction asymptotically approaches the similarity solution defined by equation (13). The constant C_1 is 0.09. This value agrees well with the experimental results given in Table 1.

The spreading rate of the propane jet is characterized by the mixture fraction half-radius R_{fh} which is defined as the radial location where the mixture fraction scalar f is half of the value on the centerline. The definition reads

$$\frac{R_{fh}}{R} = C_2 \left[x - x_{0,2})/R\right], \qquad (14)$$

where C_2 is the centerline decay constant and $x_{0,2}$ is a virtual origin. The present LES predicts the spreading as $C_2 = 0.06$ (Fig. 5). The spreading rate is compared with the experimental findings in Table 1 and again, the agreement is excellent.

More detailed information on this validation case can be found in Renze et al. (2008).

COMPUTATIONAL DETAILS AND CONSTRAINTS

The simulations have been conducted on two block structured grids, one for the first part of the nozzle (grid A), covering the region upstream of $x \approx 3.5mm$, and the other mesh encompasses the part downstream of this point (grid B). Only one out of the six injection holes is taken into account. That is, the spanwise diameter is reduced from $15mm$ to $1.8mm$, i.e., the distance inbetween two injection holes, and the spanwise boundaries are considered periodic. The upper and lower wall boundary layers are neglected such that an Euler boundary condition is introduced.

These latter measures for the vertical and spanwise direction are taken to significantly reduce computational costs. The purpose of the splitting in two smaller instead of one large grid also is efficiency since downstream of the throat the mesh can be coarsened to reduce the number of grid

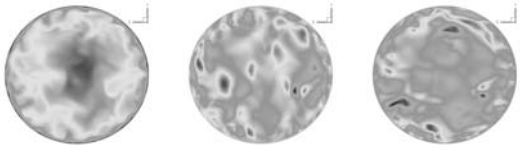

(a) streamwise direction (b) y-direction (c) z-direction

Figure 6: Distribution of the velocity components of the turbulent flow field in the injection pipe

points. The injector geometry, in particular the injection hole, makes a complex grid structure necessary. This results in a high number of grid points normal to the nozzle-centerline. The supersonic nature of the flow downstream the nozzle throat and the omitted boundary layers allow a simple coupling of two simulations, therefore the second nozzle part can be meshed using a simple H-grid. This saves an immense amount of grid points, resulting in a reduced computational time.

The aforementioned block structured grids consist of 24 blocks. Grid A has 24 million grid points (Fig. 7), grid B 50 million points (Fig. 8). The minimum grid spacing is reached at the upper and lower edges of the injector's blunt trailing edge with $\Delta x_{min} = 5 \times 10^{-6} m, \Delta y_{min} = 1 \times 10^{-6} m, \Delta z_{min} = 1 \times 10^{-5} m$, which corresponds to $y^+ = 1$. Near the centerline the grid stretches to $\Delta x^+ = 60, \Delta y^+ = \Delta z^+ = 30$.

The flow through the injection pipe at a Reynolds number of almost $Re = 16000$ is considered to be fully turbulent. Therefore, grid A includes a pipe grid with about 2.5 million grid points that is used to generate a turbulent pipe flow. A periodic boundary condition for the velocity field is used to generate a turbulent flow in the injection pipe. Figure 6 shows the instantaneous flow field in the injection pipe which is connected via a slicing method with the main flow (Rütten et al. 2001).

Grid A and grid B are connected using a supersonic outflow boundary condition. The instantaneous flow data is stored and then interpolated to fit the inflow plane of grid B. An expanded supersonic inflow condition allows for the resulting interpolated data. The quadruple time-step of grid A is used for the simulation of grid B.

RESULTS AND DISCUSSION

Dominant Flow Structures

The flow in the area downstream of the injector is dominated by strong vortex shedding at the injector's blunt trailing edge. The observed Strouhal number is $Sr \approx 0.2$. The simulations show these primary vortices to be preserved throughout the whole nozzle. Unfortunately, the observed vortices confine most of the injected TEOS mass, and hence impede any strong mixing process. The resulting temporal TEOS distribution is very inhomogeneous, whereas the time averaged spatial TEOS distribution is acceptable. A reason for this behavior might be the favorable pressure gradient in the Laval-nozzle. In the case of an adverse pressure gradient the vortices would probably break down and the mixing process would be enhanced.

Turbulence Analysis

Figures 9 to 11 show the development of the turbulence

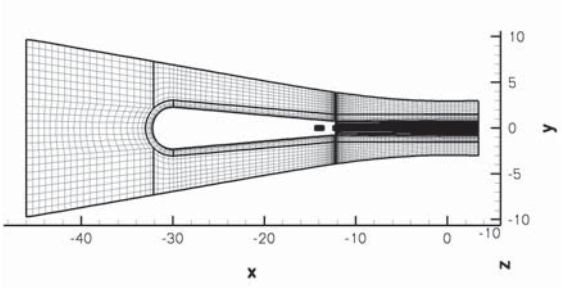

(a) X-Y-cut-plane in the nozzle center, the injector profile is visible in the center, every fourth grid point shown

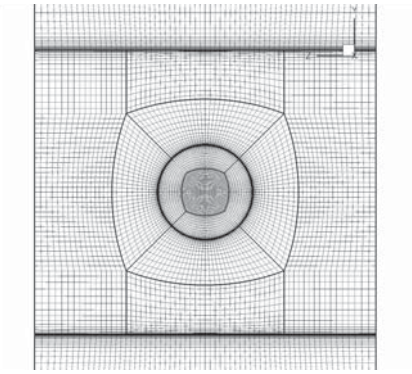

(b) Cross-section at the injector base, every second grid point shown

Figure 7: Grid A

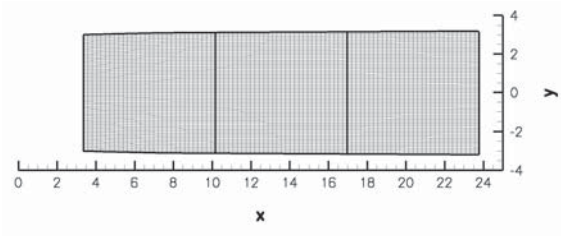

(a) X-Y-cut-plane in the nozzle center of the first 3 out of 24 blocks of grid B, every fourth grid point shown

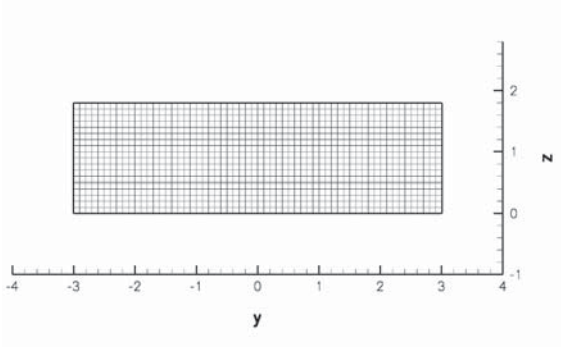

(b) Cross-section at the upstream end of grid B, every fourth grid point shown

Figure 8: Grid B

structure using the anisotropy-invariant map of Lumley and Newman (1977). The origin of the map defines isotropic turbulence. The other two vertices represent isotropic two-component turbulence (left vertex) and one-component turbulence (right vertex). The curve connecting the origin and

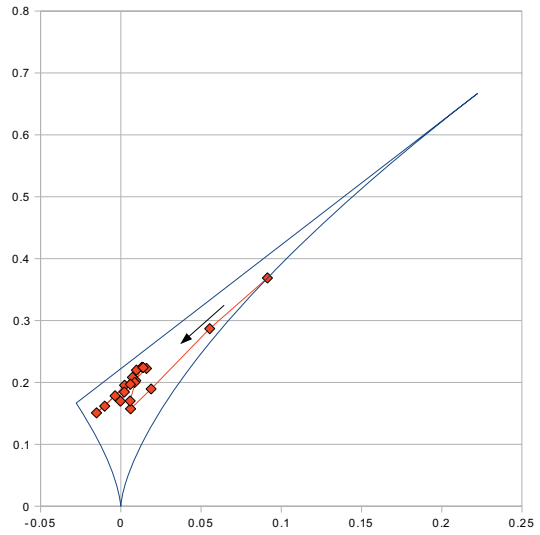

Figure 9: Lumley-Newman map depicting the turbulence anisotropy along line I, the arrow denotes the order in flow direction

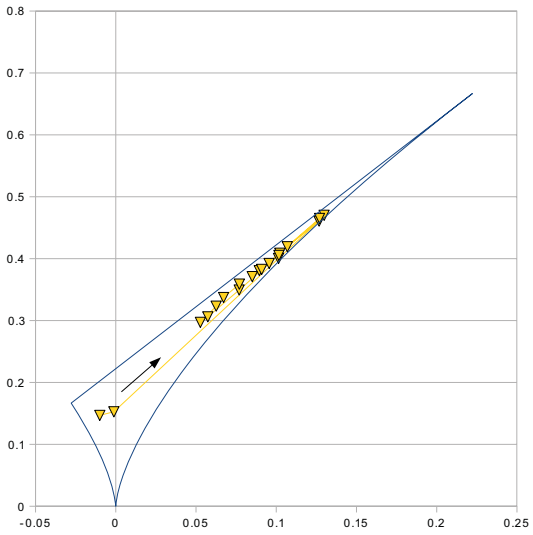

Figure 10: Lumley-Newman map depicting the turbulence anisotropy along line II, the arrow denotes the order in flow direction

the left vertex defines axisymmetric turbulence the statistical properties of which are invariant under rotation around one axis with fluctuation intensities along the axis of rotation being smaller than in the remaining directions. The curve between the origin and the right vertex represents axisymmetric turbulence with fluctuation intensities along the axis larger than in the other directions. The connection of the left and the upper vertex defines two-component turbulence.

The symbols inside this Lumbley-Newman map in figure 9 describe the variation of the turbulence character along a straight line in the streamwise direction which originates just downstream of the edge of the blunt injector trailing edge (line I), at $y = \pm 0.75mm$. In the immediate vicinity of the injector the flow field still possesses the structure of one-component turbulence. Further downstream the character changes from axisymmetric turbulence with a pronounced fluctuation in the streamwise direction to isotropic two-component turbulence. The latter structure is observed $\Delta x = 24 D_{te}$ downstream of the injector's trailing edge.

Figure 10 depicts the Lumley-Newman map including data of line II, which follows the nozzle centerline for the aforementioned $24 D_{te}$ downstream of the injector's trailing edge. In contrast to line I the turbulence character in the injector vicinity is close to isotropic two-component turbulence and changes towards axisymmetric turbulence with pronounced fluctuation in the streamwise direction, which is the inverse development compared to line I.

Figure 11 describes the turbulence character along line III, which connects the aforementioned lines I and II about $\Delta x = 1.2mm = 0.8 D_{te}$ downstream the injector trailing edge. Even this close to the trailing edge the turbulence character at line I as well as at line II tends towards the state it has far downstream, i.e., at line I the pronounced one-component axisymmetric turbulence almost vanished and at line II the isotropic two-component turbulence developed towards axisymmetric turbulence with pronounced streamwise fluctuations. The transition inbetween these states along line III is of linear character.

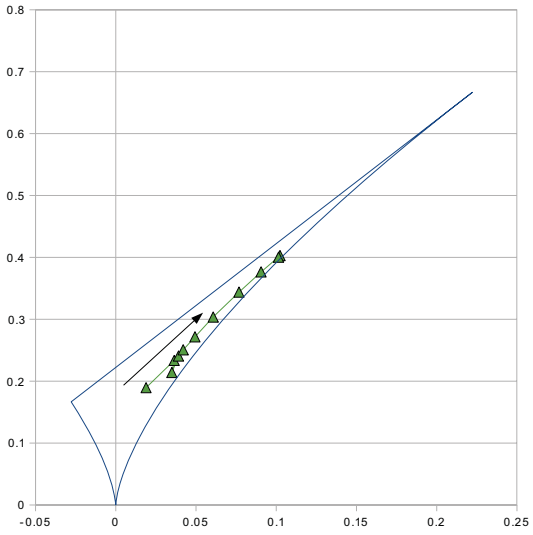

Figure 11: Lumley-Newman map depicting the turbulence anisotropy along line III, the arrow denotes the order from line I to line II

CONCLUSION

The presented results show that the current injector configuration is not able to perform a homogeneous temporal mixture of TEOS with the co-flow. The strong primary vortices shedding from the blunt injector trailing edge confine most of the injected mass flux and the favorable pressure gradient impedes vortex break down. The turbulence structure of the wake is two-dimensional which is a further indicator for poor mixing quality.

To generate a more isotropic turbulence and improve the mixing quality it is necessary to generate turbulence in span-

wise direction. Ramps, similar to those used at SCRAMJET injectors, or other types of vortex generators, could be used to induce longitudinal vortices and improve mixing quality, as observed by Gerlinger et. al (2008). The effectiveness of this approach for an accelerated nozzle flow will be subject of future investigations, as well as other adjustments to nozzle and injector configuration.

ACKNOWLEDGEMENTS

The support of this research by the Deutsche Forschungsgemeinschaft (DFG), via the project "Gasdynamically Induced Nanoparticles", and by the High Performance Computing Center Stuttgart (HLRS) is gratefully acknowledged.

REFERENCES

Berglund, M., and Fureby, C., 2007, "LES of supersonic combustion in a scramjet engine model", *Proceedings of the Combustion Institute*, Vol. 31, Issue 2 , pp. 2497-2504.

Bogey, C., Bailly, C., and Juve, D., 2002, "Noise investigation of a high subsonic, moderate reynolds number jet using a compressible large eddy simulation", *Theor. Comput. Fluid Dyn.*, Vol. 16, pp. 273-297.

Cook, A.W., and Cabot, W.H., 2005, "Hyperviscosity for shock-turbulence interactions", *Journal of Computational Physics*, Vol. 203, pp. 379-385.

Fiorina, B., and Lele, S.K., 2007, "An artificial nonlinear diffusivity method for supersonic reacting flows with shocks", *Journal of Computational Physics*, Vol. 222, pp. 246-264.

Fureby, C., and Grinstein, F., 1999, "Monotonically integrated large eddy simulation of free shear flows", *AIAA JOURNAL*, Vol. 37, No. 5.

Gerlinger, P., Stoll, P., Kindler, M., Schneider, F., and Aigner, M., 2008, "Numerical investigation of mixing and combustion enhancement in supersonic combustors by strut induced streamwise vorticity", *Aerospace Science and Technology*, Vol. 12, Issue 2, pp. 159-168.

Grinstein, F., and Fureby, C., 2002, "Recent progress on MILES for high reynolds number flows", *J. Fluids Eng.*, Vol. 127, pp. 848861.

Grzona, A., Weiß, A., Olivier, H., Gawehn, T., Gülhan, A., Al-Hasan, N., Schnerr, G.H., Abdali, A., Luong, M., Wiggers, H., Schulz, C., Chun, J., Weigand, B., Winnemöller, T., Schröder, W., Rakel, T., Schaber, K., Goertz, V., Nirschl, H., Maisels, A., Leibold, W., and Dannehl, M., 2007, "Gas-phase synthesis of non-agglomerated nanoparticles by fast gasdynamic heating and cooling", *Proceedings 26th International Symposium on Shock Waves (ISSW26).*

Lumley, J.L., and Newman, G.R., 1977, "The return to isotropy of homogeneous turbulence", *J. of Fluid Mechanics*, Vol. 82, pp. 161-178.

Peyret, R., and Taylor, T.D., 1983, "Computational methods for fluid flow", *Springer.*

Renze, P., Schröder, W., and Meinke, M., 2008, "Large-eddy simulation of film cooling at density gradients", *Int. J. Heat Fluid Flow*, Vol. 29, pp. 1834.

Rütten, F., Schröder, W., and Meinke, M., 2005, "LES of low frequency oscillations of the dean vortices in turbulent pipe bend flows", *Physics of Fluids*, Vol. 17, Issue 2, 035107.

Schefer, R.W., Dibble, R.W., 2001, "Mixture fraction field in a turbulent non-reacting propane jet", *AIAA Journal*, Vol. 39 (1), pp. 64-72.

Schild, A., Gutsch, A., Mühlenweg, H., Pratsinis, S. E., 1999, "Simulation of nanoparticle production in premixed aerosol flow reactors by interfacing fluid mechanics and particle dynamics", *J. Nanoparticles Res. I*, pp. 305-315.